PHYSICAL REVIEW B VOLUME 50, NUMBER 19 15 NOVEMBER 1994-I

Focusing and defocusing in electron scattering along atomic chains

S. Valeri, A. di Bona, and G. C. Gazzadi
Dipartimento di Fisica and Unità INFM, via Campi 213/a, 41100-Modena, Italy
(Received 30 June 1994)

We investigated the degree of forward focusing and of multiple-scattering-induced defocusing for electrons in the keV range along regular chains of different atomic density in GaAs and GaP single crystals. The intensity angular anisotropy of elastic and inelastic (losses) Auger electrons was measured in the primary-beam diffraction-modulated electron-emission approach. In variance to the photoelectron-diffraction (PD) case, the possible influence of the energy-loss mechanism on the observed anisotropy can be disregarded and the in-depth distribution of the scattered intensity is independently determined. Both the focusing and defocusing lengths were found to be significantly larger than in previously reported PD results, and strongly dependent on the interatomic spacing. A comparative study of defocusing along the Ga [110] chains in GaAs and GaP gives experimental evidence of the influence of nearest-neighbor atomic rows (As and P, respectively) on the scattering processes.

The role and importance of multiple-scattering (MS) processes in spectroscopies based on electron scattering and interference has been widely recognized.[1-5] Although in the high-electron energy range (>500 eV) diffraction maps can be described to a first approximation by a single-scattering (SS) kinematical approach, MS has been found to significantly affect the intensity anisotropy.[3,4,6-9] In this energy region, the angular distribution of the scattered intensity is mainly determined by the high directionality of the elastic-scattering cross section (forward focusing effect), resulting in a strong angular modulation with maxima along the interatomic axes. The angular distribution of photoelectron and Auger electron intensities thus directly reflects the local order at the emitter site, and this makes the photoelectron-diffraction (PD) and Auger electron-diffraction (AED) techniques appealing for easy and direct determination of local structures.

When the scattering-interference process is experienced by the incoming electron beam, the incident-wave amplitude is spatially modulated within the solid resulting in a marked dependence of the whole secondary electron emission (true secondary, elastic and inelastic Auger electrons, elastically and inelastically backscattered electrons) on the incidence angle [primary-beam diffraction-modulated electron emission (PDMEE)].[9-12] A constant takeoff angle,[11] or a sufficiently high degree of analyzer angular integration[10,12] is necessary to avoid the superposition of outgoing electron-diffraction effects.

In both PD/AED and PDMEE, a significant defocusing occurs as a result of MS along atomic chains. In essence, in the presence of additional scatterers, the scattering electron is further deflected to directions other than forward, and this process may weaken and even destroy the anisotropy along atomic chains. The SS theory disregards this effect because it is related to higher-order scattering events. As a consequence, although SS theory correctly describes the positions of maxima and minima in the intensity angular distribution of PD/AED and PDMEE experiments, a MS approach is required to account quantitatively for the observed anisotropies. A randomization by MS would be very appealing, e.g., to improve surface sensitivity for assessing surface reconstruction.[13] A narrowing of forward focusing peaks also results from MS, thus improving angular resolution.[4,14]

The defocusing of scattering intensity along linear chains of atoms has been studied theoretically by Tong, Poon, and Snider.[1] Later, SS and MS calculations were comparatively carried out, to clarify the dependence on the material and on the chain structure.[3,4,6,15] It has been shown that the addition of a second scatterer does not necessarily lead to a decrease in the anisotropy. For the Cu and Al (011) linear chains,[15] the calculations predict an effective focusing up to three to five atoms in the row, and a steep defocusing when more atoms are added. It has been reported that six to eight atoms in the line are enough to completely suppress the forward-scattering intensity from one emitter.

The direct experimental evaluation of the defocusing length was first done using thin-film epitaxy.[3,7,14] However, a proper interpretation of these results depends on a sharp and well-characterized interface, a condition that is not always fulfilled. An alternative approach was recently suggested, based on the differences in the experimental diffraction patterns of elastically and inelastically (losses) scattered photoelectrons.[16-18] These differences were ascribed to the different relative importance of MS, owing to the different probing depths. Therefore, the comparison between the angular anisotropy of core photoelectrons and that of the corresponding plasmon-loss satellites became a very popular and widely used approach to investigate the dependence of PD defocusing along atomic chains on the material, the length and the internal structure of the chain, and on the kinetic energy (KE) of the scattering electrons.[19-21] The results show that the "intuitive" picture of focusing-defocusing does not describe the generality of the experimental findings. In particular, it has been shown that the internal structure of the chains plays a decisive role[19,21] and that the defocusing length is much larger than theoretically predicted.[20,21] With this respect a significant result has been recently reported, based on surface-sensitive secondary-electron-imaging (SEI) measurements, which does not involve inelastic scattering.[22] It was shown that even when

0163-1829/94/50(19)/14617(4)/$06.00 ©1994 The American Physical Society

the electrons scatter from up to 11 atoms in a regular row, they remain focused and it was suggested that in the energy-loss-based PD experiments the energy-loss mechanism acts as a distinct and independent source of anisotropy reduction because the plasmon creation partially destroys the coherence of the photoelectron wave.

The PDMEE technique enabled us to bypass this bottleneck. In fact, in this approach, all the features in the energy-distribution spectrum are simply used as fingerprints of the occurrence and strength of the focusing-defocusing processes, which are actually experienced by the primary, exciting wave. Therefore, the angular anisotropy of the primary wave amplitude at the emitting sites is totally reflected in the intensity anisotropy of both elastically *and inelastically* emitted electrons.[10] The order of plasmon loss an Auger electron has undergone can be associated with its mean depth of origin. Therefore, we measured a selected set of elastic and inelastic Auger features to probe focusing-defocusing over a considerable chain length. Different energies of the primary beam were used. In fact an additional advantage of PDMEE is the possibility to vary independently the KE of the scattering electrons, while, in PD, changes in the photoelectron KE also result in different sampled depths via the energy dependence of the inelastic mean free path. With respect to the SEI approach, PDMEE offers the advantage of chemical selectivity providing that chemically identified features (Auger peaks and losses) in the energy distribution are monitored. We were, therefore, able to investigate specific atomic chains in different environments. Finally, we also modeled the processes in a rather simple way to get insight on the in-depth efficiency of the focusing-defocusing process.

Measurements were performed on the GaAs and GaP (110) surface exposed by cleavage in UHV ($<2\times10^{-10}$ torr). The electron energy distributions were recorded by a cylindrical mirror analyzer (CMA) operating at 0.3% resolution in the first derivative mode. The coaxial electron gun was used as exciting source, at a beam energy E_p of 2 and 3 keV and a beam current of 500 nAmp. The Ga MMM and LMM Auger peaks were recorded, at 55 and 1070 eV, respectively. The first bulk plasmon-loss feature associated to the MMM peak was also monitored, while for the LMM peak both first and second bulk plasmon peaks were recorded. The escape depth was evaluated, on the basis of the Seah and Dench formula,[23] to be 7 and 26 Å for the 55 and 1070 eV "elastic" electrons, respectively, in GaAs. To a first approximation, the plasmon creation can be regarded as an independent process governed by the Poisson distribution and the electron inelastic mean free path substantially coincides with the plasmon-creation length.[16] In this assumption, the electrons in the first and second bulk plasmon come from a mean depth two and three times larger than the escape depth of the corresponding elastic Auger emission. Therefore, the anisotropy can be checked up to a depth of about 80 Å. The peaks and losses intensity was evaluated as the peak-to-peak height of the derivative spectrum. On GaAs, the MNN (31 eV) and LMM (1228 eV) As Auger peaks were also measured, together with the first bulk plasmon feature associated to the As LMM peak.

The incident beam was scanned in the plane containing the [110] and [1$\bar{1}$0] directions by rotating the sample in front of the CMA, over an angular range of 90°, which contains the [110], [100], and [3$\bar{1}$0] axes. We will refer in the following to this plot as [1$\bar{1}$0] plot. The incidence angles are measured with respect to the surface normal: positive and negative values refer to the [1$\bar{1}$0] and [$\bar{1}$10] azimuths, respectively. The transmission of the analyzer is independent on the sample orientation in the angular range we explored, as checked by a separate experiment on an amorphous surface. The CMA was found to provide a degree of integration over the takeoff angle sufficient to smear out the diffraction effects of the outgoing electrons.[10,24]

The low- and high-energy region of the GaAs Auger spectrum are shown in Fig. 1(a), for 3-keV electrons at normal incidence. The relevant peaks and losses are labeled. In Fig. 1(b), the Ga MMM, Ga, and As LMM, and Ga LMM-related bulk plasmon intensity is shown, as a function of the incidence angle. The number and angular position of the relevant features are strictly similar. Intensity enhancements occur in correspondence of low-index directions encompassed in the [1$\bar{1}$0] scan. Other

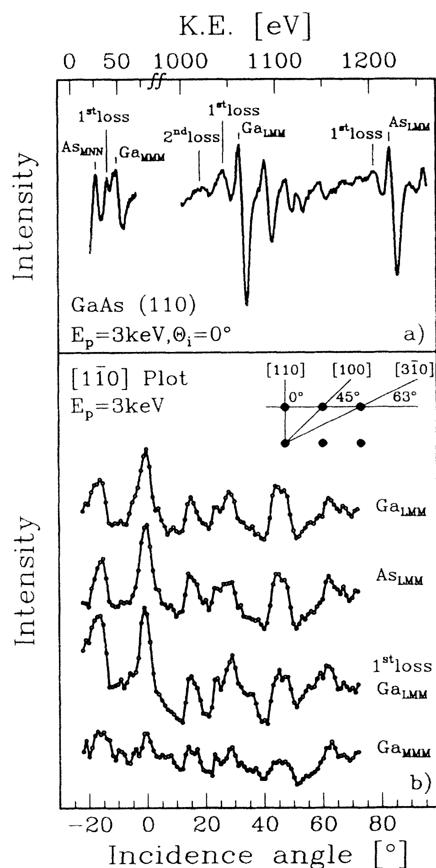

FIG. 1. (a) First derivative of the energy distribution of Ga and As Auger electrons from the GaAs(110) surface. (b) Angular intensity distribution of Ga and As LMM peaks, of Ga LMM-related first bulk plasmon, and of Ga MMM peak. Main crystal axes encompassed in the [1$\bar{1}$0] plot are also sketched.

relevant features are related to higher-order interferences. The similar angular behavior of signals of very different KE unambiguously indicates that we are only dealing with a primary electron-scattering-interference process, with a negligible, if any, contribution from diffraction of escaping electrons. The intensity angular-distribution curves of Fig. 1(b) only differ in the absolute value of the anisotropy. The anisotropy is defined as $2(I_{max}-I_{min})/(I_{max}+I_{min})$, where I_{max} and I_{min} are the maximum and minimum intensity of a selected feature in the plot. Differences in the anisotropy between Auger peaks of different KE, and between elastic and inelastic Auger electrons, stem from two distinct and independent effects, both related to the different sampled depth: (i) the relative importance of the isotropic contribution from the outermost layer to the overall intensity, and (ii) the in-depth anisotropy profile due to the interplay between the focusing and defocusing effects. The first contribution can be separately determined within a simple attenuation model, enabling an appropriate correction to be applied to the measured anisotropy to isolate the second contribution.

The anisotropy values for the 0° feature in the angular intensity distribution of Ga peaks and plasmon losses are shown in Fig. 2 for $E_p=3$ keV, as a function of the mean depth of origin. The results of three different runs, which coincide within the experimental error, are reported. Results relative to the As signals are also shown, which satisfactorily match the trend of the Ga values, as expected on the basis of the strong similarity in scattering efficiency and of the equivalence of atomic position of Ga and As in GaAs along the $[1\bar{1}0]$ azimuth. The anisotropy sharply increases between 7 and 35 Å, then smoothly decreases.

A numerical modeling of the experimental results has been performed assuming the primary wave intensity anisotropy to have the in-depth distribution sketched in the inset of Fig. 2. The zero value between $z=0$ and z_0 accounts for the isotropic contribution of the outermost layer, then the anisotropy linearly increases between z_0 and z_1 up to a maximum value A_{max}. Between z_1 and z_2 the anisotropy remains constant, and finally linearly decreases down to zero between z_2 and z_3.

The measured anisotropy of an emitted signal can be regarded as the sum of the subsurface layer contributions to the total intensity weighted by the local anisotropy of the primary beam

$$A=\int_{z_0}^{z_3}\frac{1}{n!}\left[\frac{z}{\lambda}\right]^n e^{z/\lambda}A(z)dz\ , \tag{1}$$

where n is the order of the plasmon loss, and λ the inelas-

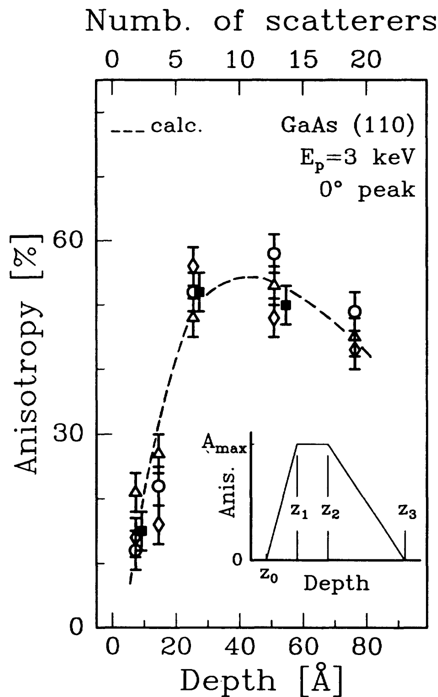

FIG. 2. Anisotropy values of the [110], 0° feature in the angular intensity distribution of Ga (open symbols) and As (■) electrons as a function of the mean depth of origin. In sequence, for increasing depth: Ga MMM, As MNN, Ga MMM-related first loss, Ga LMM, As LMM, Ga LMM-related first loss, As LMM-related first loss, and Ga LMM-related second loss. Dashed line is a fit of the experimental data calculated assuming the anisotropy profile sketched in the inset: z_1, z_2, z_3, and A_{max} are the fitting parameters.

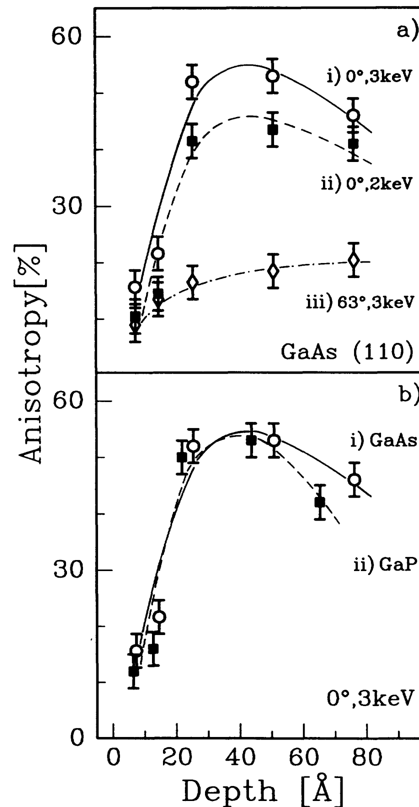

FIG. 3. Anisotropy values in the angular intensity distribution of Ga electrons as a function of the mean depth of origin, for different values of *Ep* [panel (a), curves (i) and (ii)], along different atomic chains [panel (a), curves (i) and (iii)] and in different materials [panel (b)]. Lines are simply a guideline for the eyes.

tic mean free path of the considered signal, and $A(z)$ is the assumed anisotropy function.

The z_1, z_2, z_3, and A_{max} parameters have been used to fit the experimental data. The best fit (dashed curve in Fig. 2) was obtained for the following values: $z_1 = 35$ Å, $z_2 = 40$ Å, $z_3 = 105$ Å, and $A_{max} = 97\%$.

These results indicate that the focusing enhancement prevails up to eight to ten scatterers along the [110] regular Ga (or As) chain, then the defocusing effect becomes dominant. However, about eight additional scatterers only reduce the anisotropy to 80% of the maximum value. For a complete defocusing a significantly higher number of atoms (of the order of 25) should contribute. These results widely extend the range over which the focusing effect has been found to persist.

The in-depth anisotropy behavior of the Ga signals is shown in Fig. 3 as a function of different parameters. The results represent average values of several runs. Changing the energy of the primary beam from 3 to 2 keV, the maximum anisotropy value also reduces, but the general shape of the in-depth anisotropy profile is preserved [Fig. 3(a), curves (i) and (ii)]. A marked dependence of the scattering processes on the electron energy has been reported in the low-energy range (< 1 keV),[17,20] while in the high-energy range, the properties of the electron-atom scattering are assumed not to change significantly with energy. Our results suggest that focusing is less effective on moving from 3 to 2 keV, whereas defocusing efficiency is nearly unaffected.

The spacing of the atoms along the regular Ga chain is a more crucial parameter. Moving from the 3.99 Å of the [110] chain ($\theta i = 0°$) to the 8.93 Å of the $[3\bar{1}0]$ chain ($\theta i = 63°$), the anisotropy profile is in fact strongly modified. The anisotropy steadily increases up to a maximum value of 20% [Fig. 3(a), curve (iii)], and the onset of the defocusing effect, if any, is located deeper than the maximum depth we monitored, indicating a reduced efficiency of both the focusing and defocusing process with respect to the [110] chain. These results are in agreement with previous reports,[4,6,22] on a significant focusing and/or defocusing decrease with increasing interatomic spacing.

It has been recently suggested that the contribution from different, not necessarily collinear atoms to the scattering processes along a specific chain should not be neglected.[22,25] Although theoretical efforts have been mostly restricted to MS in single isolated rows, calculations including MS effects between adjacent rows have been sometimes reported, which are assumed to produce more realistic results.[3,26] In Fig. 3(b), the anisotropy values of the 0° feature in the Ga peak and losses intensity angular distribution for GaAs and GaP (110) surface are shown, at $E_p = 3$ keV. The atomic spacing along the Ga [110] chains in the two crystals is similar (3.99 and 3.85 Å for GaAs and GaP, respectively). The GaAs and GaP results show a small but definite difference, that can be unambiguously ascribed to the effect of the different neighboring rows (As and P, respectively). A larger defocusing efficiency seems to occur in GaP. This is the first direct, experimental evidence of the importance of nearest-neighbor atomic chains in the defocusing processes. We are not aware of any theoretical calculations that include such an effect, however, it is not unreasonable to assume that large changes in the surrounding scattering potentials modify MS effects.

We conclude that (i) forward focusing of keV electrons is enhanced along atomic rows up to more than ten scatterers, then defocusing occurs, over a length much longer than previously reported; (ii) efficiency of both focusing and defocusing processes decreases with increasing interatomic spacing in the chain; (iii) it has been shown that the contribution of neighboring chains to the scattering cannot be neglected.

The authors are indebted to E. Angeli for valuable technical support. This work is part of the Progetto Finalizzato "Materiali Speciali per Tecnologie Avanzate" of CNR, Italia, and was supported under Contract No. 93.01234.PF 68. Financial support from MURST is also acknowledged.

[1] S. Y. Tong *et al.*, Phys. Rev. B **32**, 2096 (1985).
[2] M. L. Xu *et al.*, Phys. Rev. B **39**, 8275 (1989).
[3] M. L. Xu and M. A. Van Hove, Surf. Sci. **207**, 215 (1989).
[4] A. P. Kaduwela, D. J. Friedman, and C. S. Fadley, J. Electron. Spectrosc. Relat. Phenom. **57**, 223 (1991).
[5] C. S. Fadley, in *Synchrontron Radiation Research: Advances in Surface Science,* edited by R. Z. Bachrach (Plenum, New York, 1992), Chap. 11.
[6] A. P. Kaduwela *et al.*, Phys. Scr. **41**, 948 (1990).
[7] W. F. Egelhoff, Jr., Crit. Rev. Solid State Mater. Sci. **16**, 213 (1990).
[8] S. A. Chambers, Surf. Sci. Rep. **16**, 261 (1992).
[9] S. Valeri and A. di Bona, La Rivista Nuovo Cimento **16**, 1 (1993).
[10] S. Valeri *et al.*, Surf. Sci. **311**, 422 (1994).
[11] S. Kono *et al.*, Surf. Sci. **287-288**, 1092 (1993).
[12] A. Stuck *et al.*, Surf. Sci. **306**, 21 (1994).
[13] M. Steelmann-Eggebert *et al.*, in *The Structure of Surfaces IV,* edited by X. D. Xie *et al.* (World Scientific, Singapore, 1994).
[14] S. A. Chambers and V. A. Loebs, Phys. Rev. B **42**, 5109 (1990).
[15] H. A. Aebischer *et al.*, Surf. Sci. **239**, 261 (1990).
[16] J. Osterwalder *et al.*, Phys. Rev. B **41**, 12 495 (1990).
[17] S. Hufner *et al.*, Phys. Rev. B **42**, 7350 (1990).
[18] G. S. Herman and C. S. Fadley, Phys. Rev. B **43**, 6792 (1991).
[19] E. Puppin *et al.*, Phys. Rev. B **46**, 13 215 (1992).
[20] W. L. O'Brien *et al.*, Phys. Rev. B **48**, 10 934 (1993).
[21] M. Seelmann-Eggebert *et al.*, Phys. Rev. B **48**, 11 838 (1993).
[22] M. Erbudak *et al.*, Phys. Rev. B **49**, 6316 (1994).
[23] M. P. Seah and W. A. Dench, Surf. Interface Anal. **1**, 2 (1979).
[24] S. Valeri *et al.*, Surf. Interface Anal. (to be published).
[25] X. Chen *et al.*, J. Vac. Sci. Technol. A **12**, 428 (1994).
[26] E. L. Bullock and C.S. Fadley, Phys. Rev. B **31**, 1212 (1985).